INFN/AE-98/23
12 novembre 1998

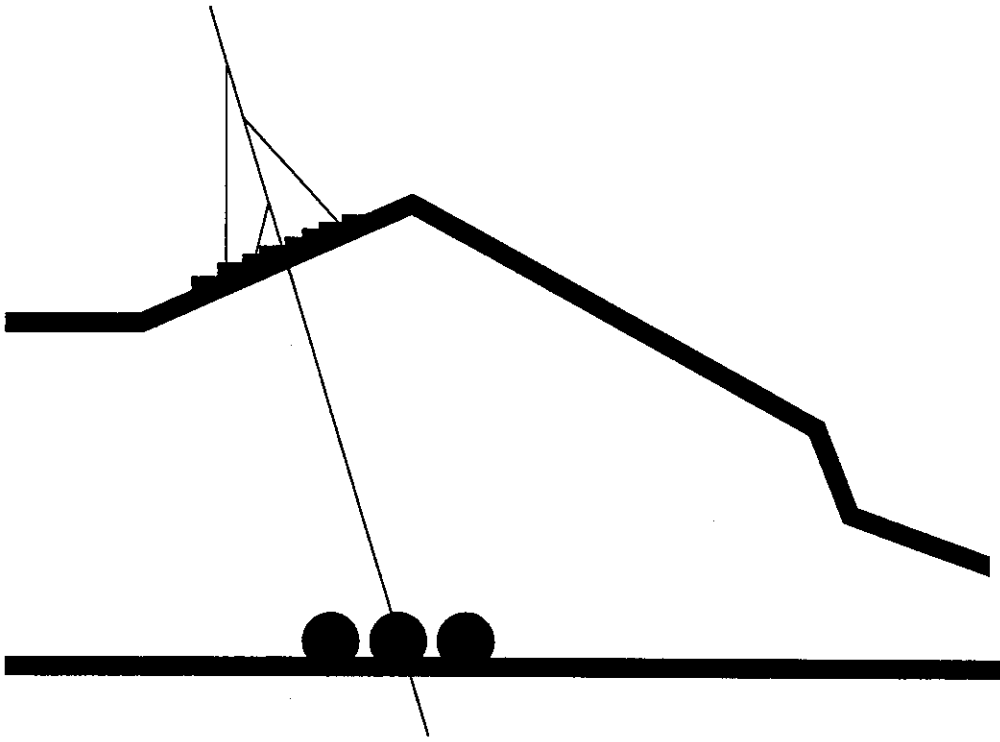

Performances of the $\simeq$ 100 kg NaI(Tl) set-up of the DAMA experiment at Gran Sasso

DAMA collaboration

also ROM2F/98/27 and submitted for publication

INFN - Laboratori Nazionali del Gran Sasso

Published by **SIS-Pubblicazioni**
dei Laboratori Nazionali di Frascati

INFN – Istituto Nazionale di Fisica Nucelare
Laboratori Nazionali del Gran Sasso

INFN/AE–98/23
12 Novembre 1998

Performances of the $\simeq$ 100 kg NaI(Tl) set-up of the DAMA experiment at Gran Sasso

R. Bernabei[a], P. Belli[a], F. Montecchia[a], W. Di Nicolantonio[b], G. Ignesti[b], A. Incicchitti[b],D. Prosperi[b], C.J. Dai[c], L.K. Ding[c], H.H. Kuang[c], J.M. Ma[c]

[a] *Dip. di Fisica, Universita' di Roma "Tor Vergata" and INFN, sez. Roma2, I-00133 Rome, Italy*
[b] *Dip. di Fisica, Universita' di Roma "La Sapienza" and INFN, sez. Roma, I-00185 Rome, Italy*
[c] *IHEP, Chinese Academy, P.O. Box 918/3, Beijing 100039, China*

Abstract

The main features of the highly radiopure $\simeq$ 100 kg NaI(Tl) set-up, searching for particle dark matter deep underground at the Gran Sasso National Laboratory of I.N.F.N, are described in some details.

1 Introduction

The main goal of the $\simeq$ 100 kg low-radioactive DAMA NaI(Tl) set-up is the search for WIMPs by the annual modulation signature [1, 2, 3] over several years, including periodical upgradings to increase its performance and sensitivity.

In the following some aspects of the competitiveness of the DAMA/NaI experiment are summarized; they are: 1) sensitivity to WIMP interaction depending and not depending on spin; 2) sensitivity to "small" (due to Na) and "large" (due to I) WIMP masses; 3) clear knowledge of the energy threshold by calibrating down to the keV range with γ sources (through a low Z window on the crystal housing) and with keV range Compton electrons; 4) suitable signal/noise discrimination profiting of the relatively high available number of photoelectrons/keV and of the different timing structures of the PMT noise pulses (single fast photoelectrons) with respect to the NaI(Tl) scintillation pulses (time distribution with time decay of order of hundreds ns); 5) absence of microphonic noise; 6) quenching factors well measured by irradiating a detector with neutrons, inducing recoils in the whole sensitive volume; 7) electromagnetic background rejection by pulse shape discrimination (PSD) and by annual modulation analysis; 8) annual modulation signature well explorable with large statistics and monitoring of several parameters.

This experiment is taking data from single photoelectron threshold to several MeV (being the optimization done for the lowest energy region: 2-20 keV) also with additional triggers to achieve some "by-product" results.

Efforts are foreseen to increase the experimental sensitivity and several upgradings are already in preparation. In particular a new R&D for further radiopurification of the NaI(Tl) is in progress with Crismatec company, planning — in case of success — to fulfil the present installation up to 250 kg.

2 Layout of the experimental set-up

The general layout of the experimental set-up is schematically shown in fig. 1.

The main parts are the shield, the Cu box containing the detectors, the NaI(Tl) detectors and the glow-box for calibrations. The detectors are enclosed in a sealed low radioactive OFHC Cu box fluxed with HP N_2 long stored deep underground; the Cu box is maintained at small overpressure with respect to the environment, such as also the glow-box. All the materials constituting the Cu box have been selected for low radioactivity by measuring with Ge detector deep underground in the Gran Sasso National Laboratory (LNGS). Results on residual radioactivity in some of the materials used in the Cu box are shown in table 1.

The Cu box maintaining the detectors in HP N_2 atmosphere assures their insulation from the environmental air, which contains Radon in traces. The ^{222}Rn ($T_{1/2}$ = 3.82 days) and ^{220}Rn ($T_{1/2}$ = 55 s) isotopes belong to the ^{238}U and ^{232}Th chains, respectively. They are in gaseous form and their daughters attach themselves to surfaces by various processes. In underground laboratories, ^{222}Rn and ^{220}Rn are due mainly to decays in the rocks and accumulate themselves in closed spaces; it is, therefore, mandatory to avoid —

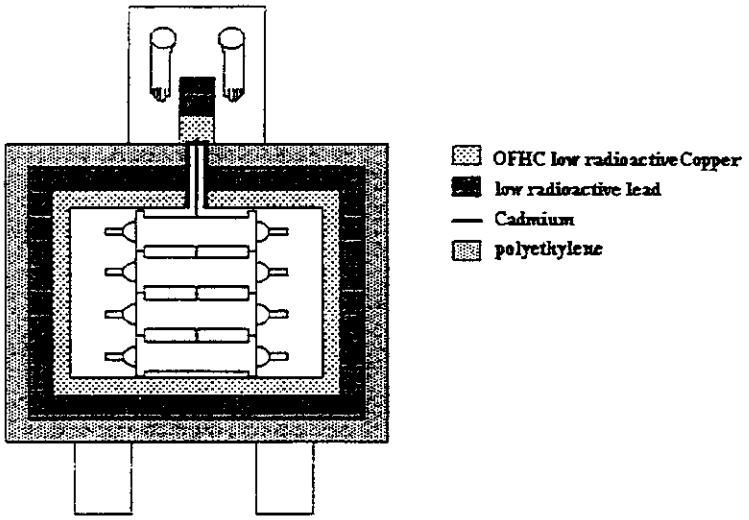

Figure 1: Layout of the experimental set-up (not in scale).

in rare event searches — any contact between the detectors and the environmental air to reduce both the background counting rate and the permanent pollution of the detector surfaces. For these reasons, Cu bricks are used at present to fulfil as much as possible the Cu box.

Table 1: Residual radioactivity in some components of the Cu box, that houses the NaI(Tl) detectors, measured at the LNGS low background facility with Ge detector; the limits are at 95% C.L.

material	^{238}U (ppb)	^{232}Th (ppb)	^{nat}K (ppm)
Cu	<0.5	< 1	<0.6
feedthroughs	—	<1.6	<1.8
Neoprene	—	< 54	< 89

The passive shield is made by 10 cm of OFHC low radioactive copper, 15 cm of low radioactive lead, 1.5 mm of Cadmium and about 10 cm of polyethylene/paraffin. The main radiopurity performances of the shield are shown in table 2. Before the use, the lead bricks have been chemically etched by HNO_3 acqueous solution, while the Cu bricks by HCl acqueous solution; the used water was extremely radiopure (produced by the BOREXINO installation [4]). An external plexiglass box is now under construction to replace the Supronyl (permeability: $2 \cdot 10^{-11} cm^2/s$[5]) envelop — fluxed with Hp N_2 — which at present wraps the shield.

The Cadmium and the polyethylene/paraffin are used to shield the set-up from environmental neutrons; the thicknesses are fixed by the available space. We take the occasion

Table 2: Measurements of the residual radioactivity in some of the components of the passive shield, performed at the LNGS low background facility by using Ge detector; the limits are at 95% C.L.

materials	^{238}U (ppb)	^{232}Th (ppb)	^{nat}K (ppm)
Cu	<0.5	< 1	<0.6
boliden Pb	<8	<0.03	<0.06
boliden2 Pb	<3.6	<0.027	<0.06
polish Pb	<7.4	<0.042	<0.03
polyethylene	< 0.3	<0.7	<2
Plexiglass	<0.64	<27.2	<3.3

to recall ref. [6], where the neutron fluxes — in the various energy regions — measured deep underground in the Gran Sasso National Laboratory are reported (see also sect. 3).

On the top of the shield a glow-box is directly connected to the Cu box, containing the detectors, through four Cu pipes. The glow box is kept in HP Nitrogen atmosphere with a small overpressure with respect to the external environment, the same as the Cu box. Source holders with O-rings can be inserted into the Cu pipes to calibrate all the detectors at the same time avoiding any direct contact with environmental air. The glow-box is equipped with a compensation chamber. When the source holders are not inserted, Cu bars fill completely the Cu pipes and seal them with O-rings; in addition 10 cm of OFHC low radioactive Cu and 15 cm of low radioactive Pb bricks are placed in correspondance of each pipe. The whole installation is under air conditioning both to assure a suitable working temperature for the electronics and to avoid any possible influence of external seasonal variations (see also sect. 9 and 10). A hardware/software monitoring system is working to offer a proper knowledge of the operating conditions; in particular, several probes are read by CAMAC and stored with the production data (see sect. 9). Furthermore, an alarm/monitoring system by self-controlled computer processes is also continuously effective.

3 The NaI(Tl) crystals

The crystals used in this set-up of $\simeq$ 100 kg NaI(Tl) [3, 7, 8] are of two kinds: 9 of them — especially realized for the experiment on annual modulation signature — have 9.70 kg (10.2 x 10.2 x 25.4 cm^3) mass and will be named in the following WIMP detectors, while 4 — previously used in another experiment — have 7.05 kg (8 x 8 x 30 cm^3) mass and will be named in the following SIMP detectors. These last ones are placed on the top, mainly to partecipate to special triggers. The detectors have been built by Crismatec company in the framework of INFN contracts. The constituting materials have been selected by using several techniques; in addition, the more effective growing procedure has been identified

and rules for handling the bare crystals have been fixed. Each detector has two 10 cm long light guides. The 9.7 kg detectors have tetrasil-B light guides directly coupled to the bare crystal (without any additional window). The 7.05 kg detectors have tetrasil-B windows; but one detector has also tetrasil-B light guides, while the others have noUV-plexiglass light guides. These detectors have the unique feature with respect to other detectors with "housings" of allowing a calibration with external γ sources down to the keV range. In fact, they have on the sealed copper housing a window made by MIB (multi interlaminar barrier): an adhesive, polyamide and high purity Al material, 168 μm thin. A MIB window is used instead of a Be window to reduce the Fe and U contaminations; it is equivalent to 500 μm of Be at energies lower than 10 keV and to 200 μm of Be for energies greater than 100 keV [9].

The first approach, in the development of highly radiopure detectors, is based on the reduction of the so-called standard contaminants: ^{40}K, ^{238}U and ^{232}Th. In fact, the first one is present at level of 0.0117% in the ^{nat}K which is very abundant in nature, while the ^{238}U and ^{232}Th have very rich chains. In table 3 we show the residual contaminations in the NaI(Tl) powder used to grow the WIMP crystals[1] as measured by techniques having different levels of sensitivity: radiopure Ge detector placed deep underground, Atomic Absorption Spectrometer (AAS) and Mass Spectrometer (MS). Moreover, we remark that the maximal sensitivity to determine the final residual contaminations is reached when directly measured in the crystal itself. In fact, the other methods are mainly limited by the radiopurity of the used set-up and geometrical efficiency (in the Ge case) or by the radiopurity of the line and added materials (in the AAS and MS case). In addition, the crystallization itself acts as a purification step, depending the reachable final levels both on the initial impurity concentrations and on the used processes.

Table 3: Measurements of the residual radioactivity in samples of the NaI powder used in the WIMP crystals growth (see text); limits are at 95% C.L.. The Ge measurements have been performed at LNGS, the AAS measurements at the chemical department of the Rome University "La Sapienza" and the MS measurements at Ispra.

Radioactive contaminant	Ge	AAS	MS
^{238}U (ppb)	< 3	—	0.56 ± 0.04
^{232}Th (ppb)	< 2.3	—	0.21 ± 0.01
^{nat}K (ppm)	<5.2	<0.8	—
^{137}Cs (ppb)	$< 2{\cdot}10^{-9}$	—	—
^{60}Co (ppb)	$(1.5{\pm}0.8){\cdot}10^{-10}$	—	—

As regards the dopant added during the growth in form of TlI, the level of residual contaminants measured deep underground at LNGS with the Ge detector was $(3 \pm 1)ppb$ for ^{238}U, $< 3ppb$ for ^{232}Th and $< 30ppm$ for ^{nat}K at 95% C.L.. We note that although

[1]However, some amount of slightly different powder has been used to fulfill the crucible in the last growth.

these results were worse than for the NaI powder (mainly as regards the ^{238}U), they were considered acceptable being the Tl content in our NaI(Tl) crystals $\simeq$ 0.1%.

Furthermore, a selection of the other materials needed to build a detector (Cu housing, teflon diffuser, glues etc.) was realized by using the Ge detector deep underground at LNGS. In table 4 the results obtained for the selected ones are shown.

Table 4: Limits on the residual radioactivity in samples of the materials used to build the WIMP NaI(Tl) detectors, as measured with the Ge detector at the LNGS low background facility. The limits are at 95% C.L.

material	^{238}U (ppb)	^{232}Th (ppb)	^{nat}K (ppm)
light guide	< 1	< 2	<1.3
glue 1	< 10	< 25	< 15
glue 2	< 5	< 8	< 6
Cu housing	< 0.5	< 1	<0.6
diffuser	< 20	< 8	< 4
low-Z window	< 0.5	< 1.2	< 300

The Kyropoulos method was chosen to produce the crystallization[2]. The crystallization process acts also as a purification step [10]; therefore measurements have been performed by using prototype crystals to determine the final level of internal residual radioactive contaminants. In particular, to determine the Potassium content measurements have been performed deep underground at LNGS inside a low background shield coupling a prototype crystal to a PMT through a standard bent light guide and fully shielding the PMT contribution with Cu bricks. The ^{40}K content has been then derived by studying the presence of the γ peak at 1461 keV. In fig. 2 the energy distribution measured there during four days is shown; no peak evidence was present and an upper limit at 95 % C.L. was derived: $^{nat}K < 50$ ppb.

A first indicative estimate of the residual U and Th contamination in a detector can be obtained by measuring the internal high energy α particles produced by both chains, profiting of the α/e pulse shape discrimination in NaI(Tl) which has in the MeV range practically 100% effectiveness. In fig. 3 we show — as a practical example — the first momentum, τ, of the time distribution for each event (as recorded by the transient digitizer), calculated within 600 ns averaging time, as a function of the energy; the two populations γ/e and α's are clearly separated. The α particles have shorter τ values.

From the number of identified α's, N_α, in a crystal of M mass during T running time, an indicative estimate of the overall U and Th residual contamination, C_{U+Th}, can be obtained by the formula $C_{U+Th} = N_\alpha/M[kg]/T[day]/5.24$ ppt, that is valid under the assumption of chains in equilibrium and of equal U and Th concentrations. In fact, under

[2]Note that this method requires a seed to grow a crystal; therefore, different quality of seeds would cause differences in the final radiopurity.

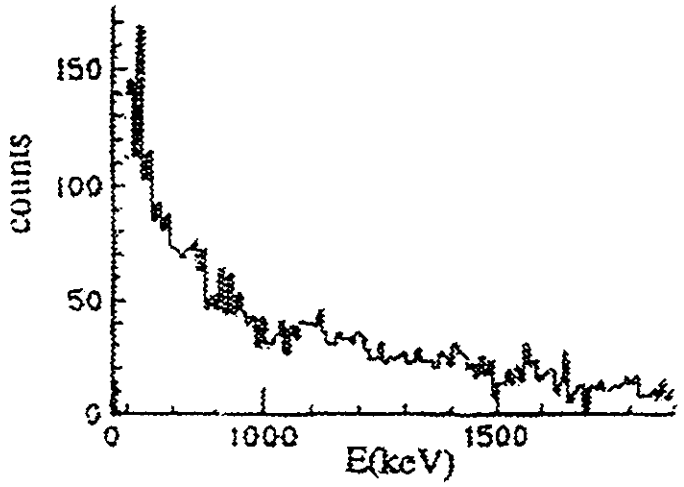

Figure 2: Energy spectrum collected with a bent light guide in order to evaluate the ^{nat}K content in prototype crystal (see text).

the assumption of equilibrium chains 1 ppt of ^{238}U gives 8.6 α/kg/day, while 1 ppt of ^{232}Th gives 1.87 α/kg/day. In table 5 we show the α content for the 9 WIMP and the 4 SIMP complete detectors some time after their arrival deep underground; the cumulative U+Th residual concentrations — estimated under the above quoted assumptions — are also shown (case a).

Another independent estimate of the ^{238}U and ^{232}Th residual contents can be obtained by studying the so-called Bi-Po events. In fact, the residual ^{232}Th internal content alone can be determined by detecting the Bi-Po events due to the ^{212}Bi β decay to ^{212}Po, which α (E_α=8.78 MeV) decays to ^{208}Pb with $T_{1/2}$ = 300 ns. Similar events can be clearly identified by the recorded pulse shapes over a 3250 ns time window (see e.g. fig. 4).

On the other hand, the residual ^{238}U internal content alone can be tagged also by Bi-Po events, due to ^{214}Bi β decay to ^{214}Po, which α (E_α=7.687 MeV) decays to ^{210}Pb with $T_{1/2}$ = 165 μs. Considering the Bi-Po events measured in the 9 WIMP crystals during 20.3 days and the proper efficiencies, we have determined 4.8 μBq/kg of ^{214}Bi and 0.42 μBq/kg of ^{212}Bi (averaged over the crystals). From the measured value for the ^{214}Bi, a contamination of 4.8 μBq/kg can be estimated also for the ^{226}Ra, that belongs to the ^{238}U chain.

On the other hand, assuming the ^{232}Th radioactive chain in equilibrium — as it is generally the case — from the measured value of ^{212}Bi, 0.1 ppt of ^{232}Th can be derived (still averaged here over the crystals). At this point, considering the ^{232}Th content determined by these Bi-Po measurements, we can recalculate in the last column of table 5 the ^{238}U content assuming again this chain in equilibrium.

To demonstrate how important is a full control of all the growth/handling parameters, we show in fig. 5 — as an example — the α distribution in the four SIMP crystals; there

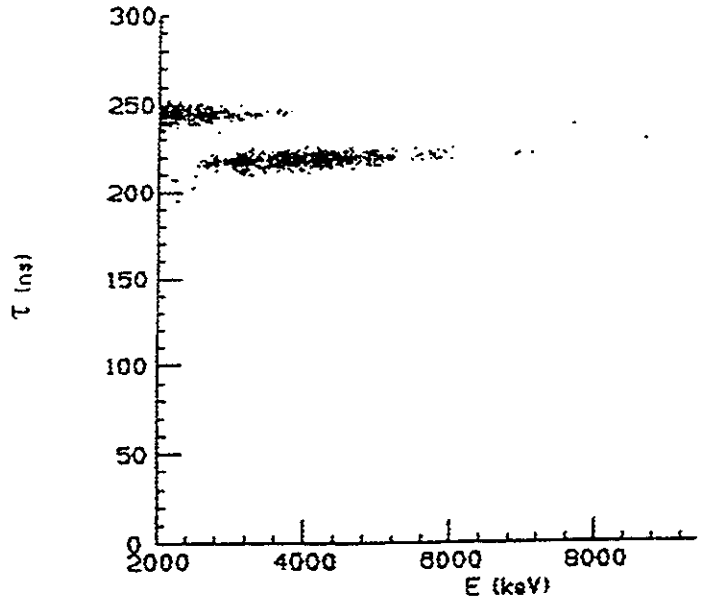

Figure 3: First momentum, τ, of the time distribution for each event (recorded by the transient digitizer) — calculated within a 600 ns averaging time — as a function of the energy in unit of keV electron equivalent. The two populations γ/e and α's are clearly separated; the α's have shorter τ's.

Table 5: The α content measured in the detectors some time after their arrival deep underground. (a) Estimate of the U+Th contamination from the α's measurements, under assumption of chains in equilibrium and of equal U and Th concentrations (see text); (b) estimate of the ^{238}U content in the 9 WIMP crystals considering the ^{232}Th content measured by the Bi-Po events (see text).

Detector on line n.	α/kg/day	case a): U+Th (ppt)	case b): U (ppt)
1	34	6.5	4.0
2	46	8.8	5.3
3	43	8.2	5.0
4	61	11.6	7.1
5	52	9.9	6.0
6	59	11.3	6.9
7	80	15.3	9.3
8	20	3.8	2.3
9	20	3.8	2.3
10	42	8.0	
11	44	8.4	
12	66	12.6	
13	60	11.5	

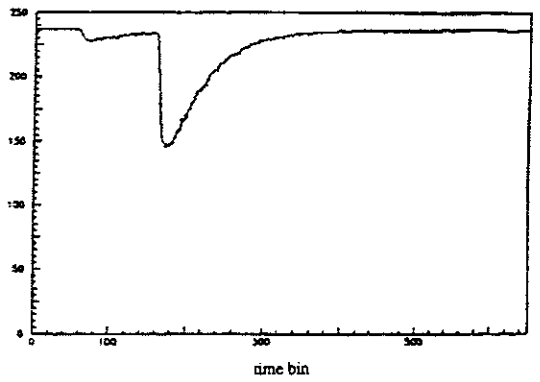

Figure 4: Typical Bi-Po event (from ^{212}Bi $\rightarrow$ ^{212}Po $\rightarrow$ ^{208}Pb) as recorded by the transient digitizer. The time bin is 5 ns.

the alpha energies are given in keV electron equivalent. As it is evident they are similar in pairs, being the only known difference in the used TlI powder[3].

As a consequence also the associated γ distribution can be expected to be different. The α peaks in the energy spectrum of fig. 5 c) — from the lower to the higher energy — can be associated with [11]: i) ^{232}Th (4.01 MeV)+ ^{238}U (4.20 MeV); ii) ^{234}U (4.77 MeV) + ^{230}Th (4.69 MeV) + ^{226}Ra (4.78 MeV); iii) ^{210}Po (5.30 MeV) + ^{228}Th (5.42 MeV) + ^{222}Rn (5.49 MeV); iv) ^{218}Po (6.00 MeV) + ^{220}Rn (6.29 MeV); v) ^{216}Po (6.78 MeV); vi) ^{214}Po (7.69 MeV); vii) ^{212}Po (8.78 MeV). This is valid also for the case of fig. 5 d) while the situation of fig. 5 a) and b) can be easily derived.

As it is clear, e.g. from table 5 and fig. 5, the residual contaminations could be significantly different even in case the detectors have been grown using the same powders and assembled with the same protocol. In fact, different casual pollutions during the growth and handling procedures are possible, being the detectors built in an industrial environment. Moreover, the uniformity of the contaminants distribution inside the total material used to construct each part of the detectors cannot be completely assured. Another additional source of differences could depend on which part of the large crystallized mass is cutted to build the detector; in fact, the purification during cristallization could not be uniform on the whole large mass grown bulk. Obviously, casual pollution could also occur by handling without the needed extreme care the detector deep underground[4].

[3]We note that no appreciable differences were seen between the two TlI used powders in the limits of sensitivity of the Ge measurements at LNGS.

[4]Furthermore, the detectors obviously do not measure only internal contaminants, but also the contribution arising from the environment; therefore, more in general, in case different installations would be used, appreciable differences in the counting rate would be found. Finally, if a detector has been exposed

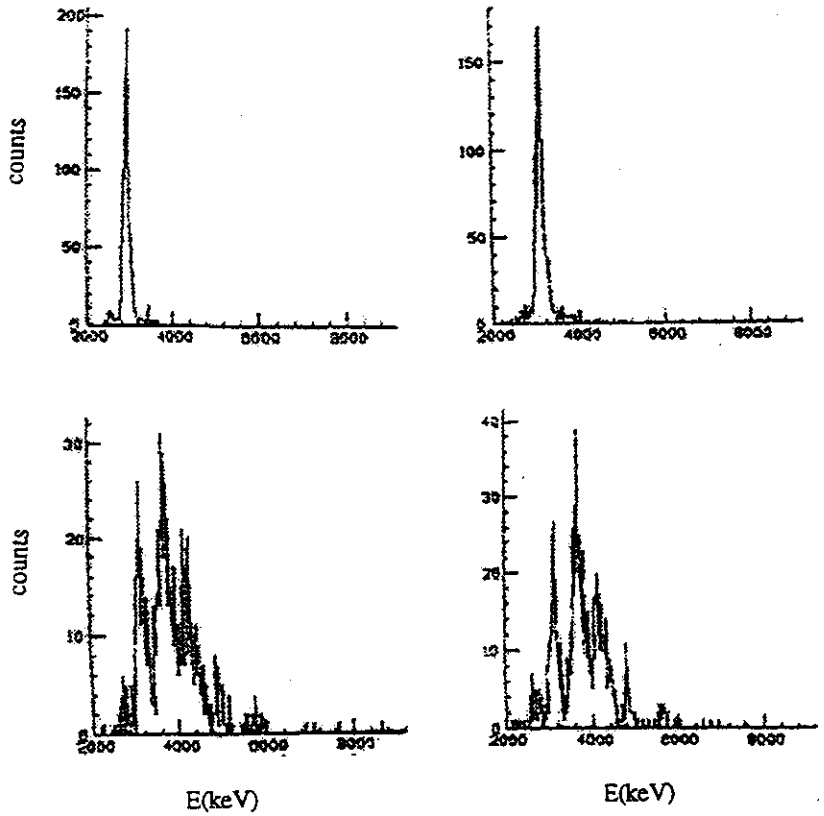

Figure 5: α energy distributions in the four SIMP crystals. The energy is given in keV electron equivalent.

As regards possible non standard contaminants, we recall that during the period of powders storage and/or crystal growing and handling at sea level (of order of at least several months for large crystals) radioactive isotopes can be produced by cosmic ray interactions. Therefore, it is good practice in this kind of experiments to wait for the decay of the short-life cosmogenic isotopes before starting the measurements. In particular, here we comment the case for ^{125}I which decays by EC to ^{125}Te giving 35.5 keV γ's and, at the same time, Tellurium X-rays and Auger electrons, whose total energy is 31.8 keV, giving rise to a peak around $\simeq$ 68 keV with half-life 60.25 days (see fig. 6). As it is evident, in this case the best situation will be reached after $\simeq$ 8 months of storage deep underground. Some arguments on cosmogenic activation in NaI(Tl) can be found in ref. [12], while the production rate of cosmogenic isotopes can be calculated mainly according to the model of ref. [13]. However, the activity of cosmogenic isotopes in NaI(Tl) detectors would be in practice generally lower than the calculated one because of purification and saturation processes during the growing procedures.

Among the possible isotopes produced by cosmogenics in NaI(Tl) [11], we point out the ^{22}Na ($T_{1/2}$=2.6 y) with calculated maximum rate level $\simeq$ 100 cpd/kg and the ^{3}H ($T_{1/2}$=14 y) with calculated maximum rate level $\simeq$ 20 cpd/kg. However, as mentioned above, in real conditions the ^{3}H activity in a NaI(Tl) detector would be essentially lower than the calculated maximum level, because it would be extracted in process of NaI(Tl) purification

to a neutron source, it and the surrounding materials have been activated.

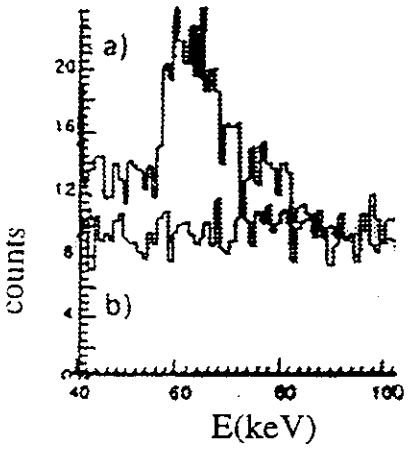

Figure 6: Energy spectrum collected at Gran Sasso with a NaI(Tl) detector just stored underground (a) and 8 months later (b). The role of $\simeq$ 68 keV peak due to ^{125}I activation (half-life 60.25 days) is evident.

and growth; therefore, rate lower than 1 cpd/kg can be expected. In our WIMP crystals an upper limit has been estimated on the ^{3}H content from the data collected in the 2-18 keV energy region [7], obtaining $< 0.9 \cdot 10^{-4}$ Bq/kg at 95% C.L.; it corresponds to $< 4.9 \cdot 10^{5}$ (95% C.L.) ^{3}H atoms in a 9.7 kg NaI(Tl) detector.

The ^{22}Na activity indeed would determine the NaI(Tl) background mainly in the high energy region: 0.5-2.7 MeV, provided that the detector is purified from standard contaminants (U, Th and K). Its activity should be close to the calculated maximum level, because its abundance does not change in process of purification and growth [5]. In our WIMP detectors an upper limit for ^{22}Na has been determined by comparing the experimental spectrum with the expected one considering the region 1700 - 2300 where the contribution from other isotopes is well reduced; it resulted to be $< 10^{-3}$ Bq/kg at 95% C.L., that is $< 10^{6}$ atoms of ^{22}Na in 9.7 kg NaI(Tl).

We recall also the possible role of the ^{87}Rb and ^{85}Kr isotopes. The ^{87}Rb isotope is a β-emitter with half-life equal to 4.8 $\cdot 10^{10}$ years and Q value equal to 273.3 keV; the presence of a ^{nat}Rb concentration at ppb level would cause $\simeq$ 70 ^{87}Rb decays/day/kg whose $\simeq$ 15% is in the 2-20 keV energy region. From the rate measured in this last energy region [7] an upper limit has been derived for the WIMP crystals to be < 0.34 ppb at 95% C.L. As regards the ^{85}Kr isotope — that could be initially present in trace in the air or in the gases used during the crystals growth and handling — it β decays (673 keV end point) 0.43% of the time to a metastable level of ^{85}Rb at 514 keV and, then, γ decays directly to the ground state with 1.46 μs lifetime. We have searched for $\beta - \gamma$ delayed coincidences with proper Δt and energies; zero events in all the 9 WIMP crystals have been found during 20.3 days and — evaluating the needed efficiency by MonteCarlo program — an

[5] The only way to remove the presence of ^{22}Na background would be the use — in the NaI(Tl) growth — of NaI powder stored deep underground.

upper limit has been set for ^{85}Kr: $< 10^{-5}$ Bq/kg at 95% C.L.

Another source of internal background, that we take into account, is the possible presence of ^{24}Na. In fact, environmental neutrons would induce the reaction $^{23}Na(n,\gamma)^{24}Na$ with 0.1 barn cross section and the reaction $^{23}Na(n,\gamma)^{24m}Na$ with 0.43 barn cross section [14]. The ^{24}Na isotope is a β emitter (end point equal to 1.389 MeV) with two prompt associated γ's (2.754 and 1.369 MeV); on the other hand the ^{24m}Na isotope decays 100% of the times in ^{24}Na by internal transition with a γ of 0.472 MeV. Comparing the typical WIMP crystal energy spectrum with the expected one, calculated by MonteCarlo code, an upper limit at 95% C.L. has been obtained for the presence of such isotopes: < 12.6 μBq/kg. Hypotizing that the production of these short-life isotopes is due to a steady thermal neutron flux, an upper limit at 95% C.L. on the thermal neutron flux can be derived: $< 5.9 \cdot 10^{-6} cm^{-2} s^{-1}$, which is well compatible with the value measured deep underground in the LNGS by ref. [6]. Obviously an analogous study can be performed pointing out the attention to the reaction $^{127}I(n,\gamma)^{128}I$; however, because of the relatively lower energy distribution of the ^{128}I decays with respect to ^{24}Na and of the uncertainties on the isomeric states, a less competitive limit would be reached. In any case, we have evaluated a limit on the ^{128m}I isomeric states [15] decays, considering that during 20.3 days three $\gamma - \gamma$ delayed coincidences — with proper energy and Δt — have been measured in the 9 WIMP crystals; it resulted < 0.16 μBq/kg at 95% C.L.

4 The photomultipliers

The photomultipliers used in this experiment have been built by EMI-Thorn.

For the first batch of PMTs, all the materials have been pre-selected by EMI, then their radiopurity has been measured at LNGS with a low background Ge. The photomultipliers are EMI9265-B53/FL, where B53 points out the use of low radioactive glass and FL that the phototube is without standard socket. They have flying leads directly connected to suitable voltage dividers with miniaturized SMD resistors and capacitors (whose low residual radiopurity has been also measured by Ge detector), mounted on thin teflon sockets; the solders were performed by using low radioactive Boliden lead and low radioactive resin. The voltage dividers have been also optimized to reach the best signal/noise ratio; a schema is shown in fig. 7.

The PMTs work near the maximum high voltage — within the linearity plateau — in order to assure a suitable energy threshold and to improve the noise rejection near it (see also sect.7).

The PMTs have nine dynods with linear focus, high quantum efficiency ($\simeq$ 30% at 380 nm), good pulse height resolution for single photoelectron pulses (peak/valley $\simeq$ 2), low dark noise rate ($\simeq$ 0.1 kHz), and a gain of $\simeq 10^6$. In the experiment each detector has two PMTs both to increase the light collection and to reduce the PMT noise contribution. They work in coincidence at single photoelectron threshold.

To measure the radiopurity of the PMT prototype — in particular as regards the ^{nat}K content — measurements have been performed at LNGS with a 3.85 kg NaI(Tl) detector,

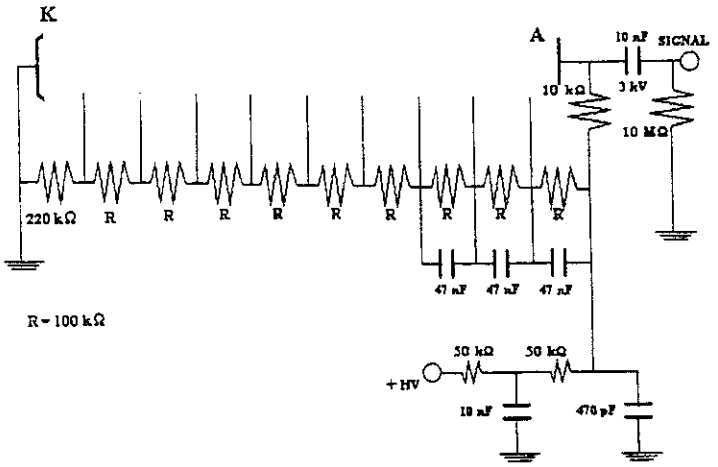

Figure 7: The voltage divider schema.

having ^{nat}K<3 ppm and U+Th <0.14 ppb; in addition, we note that it had its own "not removable" light guide made by 1" undoped NaI. Measurements with and without an additional standard bent light guide (that is shielding and not shielding the PMT contribution to the counting rate with Cu bricks) have been performed. A standard subtraction procedure of the two spectra singled out the PMT contribution in the interesting energy region as shown in fig. 8.

From these data 200 cpd have been ascribed to the 1461 keV full energy peak of ^{40}K from the PMT; then, considering the PMT as composed by a homogeneous mass of 150 g and the detector peak efficiency, a residual contamination of $\simeq$ 40 ppm in ^{nat}K has been estimated. This result - checked over a sample of 5 PMTs - was largely consistent with the radiopurity later declared by EMI for the first batch of this type of photomultipliers: ^{nat}K = (60$\pm$15) ppm, ^{232}Th = (30$\pm$10) ppb, ^{238}U = (30$\pm$20) ppb. However, we mention that in some subsequent realizations these levels were reached only for the glass, while the inner ceramics had potentially higher residual contaminations, typically: $\simeq$ 20 to 200 ppm for ^{nat}K, $\simeq$ 40 to 150 ppb ^{232}Th and $\simeq$ 40/80 ppb for ^{238}U.

In order to reduce the PMT contribution to the background at very low energy a 3" diameter 10 cm long UV Tetrasil-B light guide has been used in the WIMP detectors (see sect. 3), acting also as optical windows. The Tetrasil-B assures both suitable low radioactivity (see table 4) and very suitable optical characteristics for the NaI(Tl) light emission, being transparent down to 300 nm. However, as a proper MonteCarlo calculation has clearly pointed out [16], the residual contribution to the measured energy spectra, arising from the PMTs, is still important in the $\simeq$ 100 kg set-up.

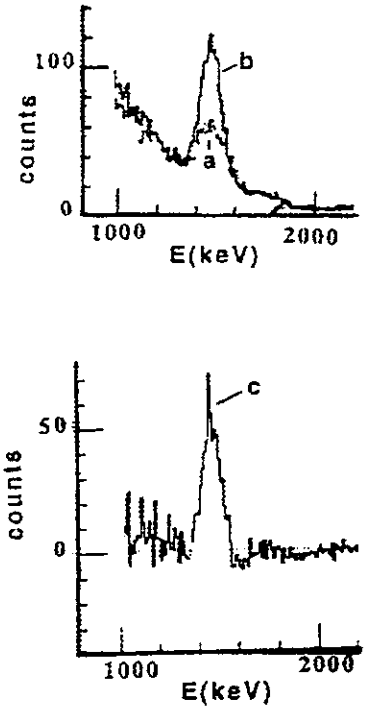

Figure 8: Energy spectra collected as described in the text: a) with standard bent light guide; b) without standard bent light guide; c) subtracted spectrum to evaluate the PMT background contribution.

5 The electronic chain

Each crystal of the set-up is viewed by two photomultipliers with grounded cathod and supplied by positive high voltage, offering the voltage suppliers a stability of 0.1%. Each photomultiplier is connected to a low noise preamplifier with a 0-250 MHz bandwidth range, with a voltage amplification of ten and with an integral linearity of $\pm 0.2\%$. Particular attention has been payed to the low voltage power system in order to limit the electronic noise.

A schematic picture of the electronic chain is shown in fig. 9.

For each detector, the signal of one PMT is processed — before entering the preamplifier — by a passive power splitter to allow the collection of the high energy signal (HE) by a CAMAC charge ADC. Then, the amplified signals of the two PMTs — by means of Linear Fan-in and Linear Fan-out — provide: i) a sum of the two pulses; ii) a signal to the charge ADC in order to record the pulse energy collected by one side only (for possible left/sum correlation analysis); iii) a signal to an analog multiplexer (piloted by

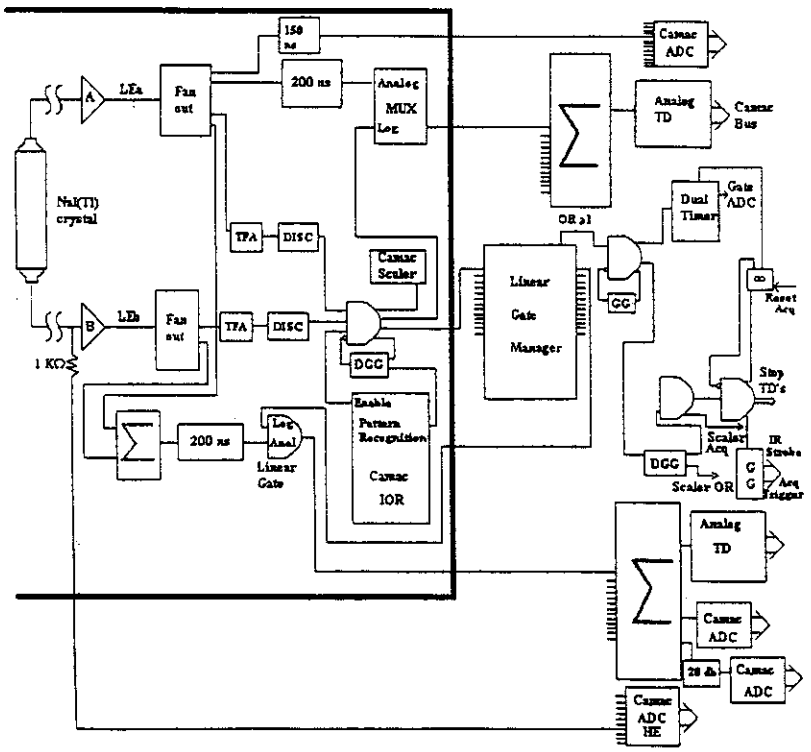

Figure 9: Schematic drawing of the electronic chain.

the trigger), whose output is recorded by an Analog Transient Digitizer (one side only); iv) the inputs of two timing filter amplifiers with 50 ns integration time.

The subsequent discriminators have triggers at photoelecton level. The detector trigger requires the coincidence of the two logical signals (see also sect. 6). A Delay Gate Generator (DGG) rejects afterglows events occurring within a time window of 500 μs after event collection; this requirement introduces a relative systematic error of $\simeq 10^{-4}$ considering that the total (from single photoelectron — that is from noise — up to "infinity") rate of single detector is $\simeq$ 0.25 Hz. The DGG gives also an input signal for a 16 bit Input/Output register (IOR) in order to single out the fired detector.

The summed signal of the two photomultipliers — delayed by a 200 ns delay cable — is sent to a linear gate, which is opened by the Linear Gate Manager (see later) in case a signal is present only in that line. In this way, only the selected line of the firing detector is addressed to: i) a Transient Digitizer (LeCroy 8828D with a digitizing sampling rate of 200 MS/s) recording the pulse shape in a 3250 ns time window; ii) a charge ADC with a scale suitable for low energy; iii) a charge ADC — after 20 db attenuation — suitable for events in the intermediate energy range. We recall that the high energy range is acquired as already mentioned above.

The total trigger is given by the OR of the triggers of the single detectors. Each single coincidence can be enabled by a CAMAC module asserting a single bit; this option is used

during calibrations to include in the total trigger a subset of the detectors. The single and total triggers are counted by means of CAMAC scalers.

The output of the coincidence gate of each detector feds the Linear Gate Manager (LGM), which produces a 4 μs gate to open the corresponding linear gate module. Furthermore, this module produces also a logic OR which generates the total trigger for the data acquisition. This allows to open the 600 ns ADC gates and to trigger the Transient Digitizers and to strobe the IOR which is also the source for the CAMAC interrupt.

A suitable circuit is used to avoid triggers during the acquisition period of an event; the corresponding dead time is evaluated by comparing the hardware triggers and the acquired triggers; it is typically of the order of a few %.

The data acquisition (DAQ) is performed by a CAMAC system, well suitable for a low-rate experiment. The DAQ system collects the pattern of the event, reading the IOR register, which represents the number of fired detectors. In case a single crystal has fired, the corresponding ADCs of the sum at low and intermediate energy, the one-side ADC at low energy and the high energy ADC are recorded. If — from the evaluation of the ADCs — the event results in the low energy range the pulse shape profiles of the sum and of the single PMT are also recorded. In case a multiple event is occurred, the pattern and all the ADCs are recorded. Every 100 events the scalers and the stability monitoring parameters are acquired. These last values are also shown and refreshed on a video screen for the operator.

Finally, we take the occasion to note that an upgrading of the electronics and of the DAQ system is in preparation in order to have in near future a transient digitizer on each detector avoiding the use of any multiplexing system.

6 Energy threshold, calibrations and efficiencies

As mentioned above, our detectors can be calibrated with external γ sources even in the keV range profiting of the MIB window; this assures a clear knowledge of the "physical" energy threshold.

It obviously depends on the available number of photoelectrons/keV; the larger is this number, the lower is the threshold. In our case the two PMTs of each detector work in coincidence at single photoelectron level, while the software energy threshold is set to 2 keV [3, 7].

The suitability of this threshold is supported by the calibrations with the ^{55}Fe source (see fig. 10), by the calibrations with Compton electrons in the keV range (see fig. 11 a), by the calibrations with the ^{241}Am source below 20 keV (see fig. 11 b) and by the measured number of photoelectrons/keV: here $\gtrsim 5.5$ depending on the detector.

The number of photoelectrons/keV has been derived for each detector from the information collected by the Transient Digitizer over the 3250 ns time window. In fact, a clean sample of photoelectrons can be extracted from the end part of this time window, where the scintillation pulses are completely ended while afterglow signals can be present. As a practical example in fig. 12 the distribution of the areas of the single photoelectron

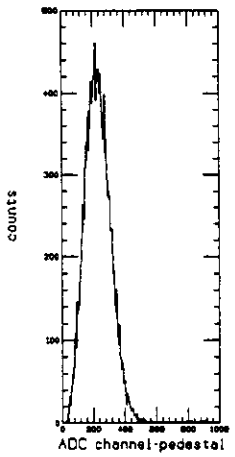

Figure 10: Energy distribution obtained by using a ^{55}Fe source on a WIMP crystal through the MIB window.

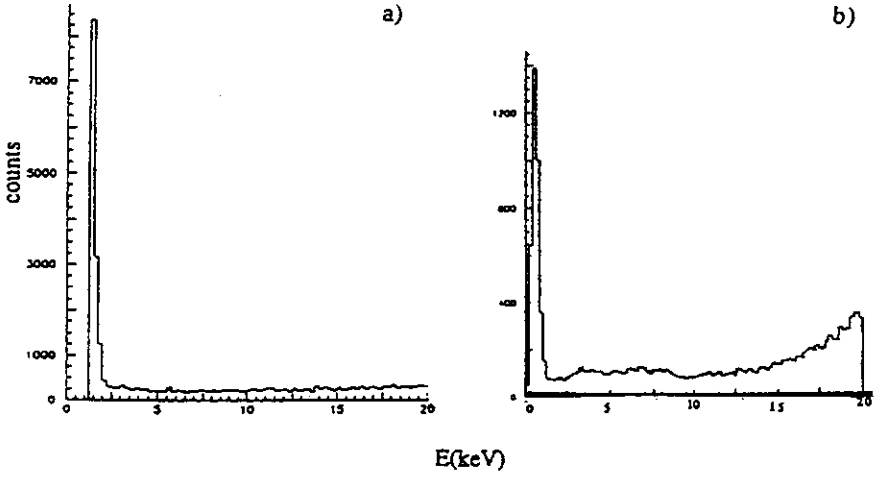

Figure 11: Examples of: a) low energy spectrum of Compton calibration with a ^{137}Cs source; b) ^{241}Am source spectrum below 20 keV.

pulses for one detector is shown. The relative peak value can be compared with the peak position of the distribution of the areas of the pulses corresponding to a full energy deposition, in the same detector, from the 59.5 keV ^{214}Am line, obtaining the number of the photoelectrons/keV searched for.

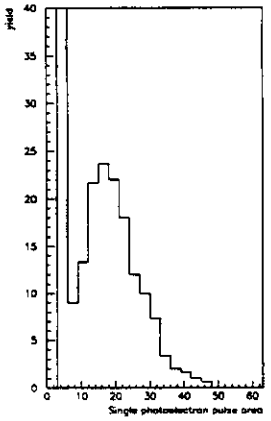

Figure 12: Typical distribution of the single photoelectron pulse area for one of our NaI(Tl) detectors.

The linearity and the energy resolution have been studied by using various sources and, in particular, in the lowest energy region mainly ^{55}Fe (5.9 keV X-rays), ^{109}Cd (22 keV X-rays and 88 keV γ line) and ^{241}Am (59.5 keV γ line) sources (see fig. 13).

As discussed in section 9 and in ref.[3, 7, 20], in running conditions the calibrations with ^{241}Am source and the information from the ^{210}Pb peak assures the proper determination of the energy calibration.

The detection efficiencies (ϵ) for photons and/or X-rays in the keV range have been measured firstly by using bare crystals, maintained in a sealed box with HP N_2 dry atmosphere because of their hygroscopicity; in particular, we mention that with a 2"·2" bare NaI(Tl) ϵ = (101±3)% was measured for the ^{55}Fe source above 2 keV and ϵ = (98±3)% for the energy interval (10-34) keV using a ^{109}Cd source. As regards the final WIMP and SIMP detectors, the measurements with ^{55}Fe source through the MIB window have given similar results when taking into account the geometry of this window. In addition, when analysing the 2-20 keV energy region in terms of WIMP-nucleus elastic scatterings, the detection efficiency to be considered is the detection efficiency for recoils; it results practically equal to unity considering the shortness of the recoil's range in matter. The absence of dead spaces in the light collection has been carefully investigated by performing suitable calibrations in different positions of the detector. This is also

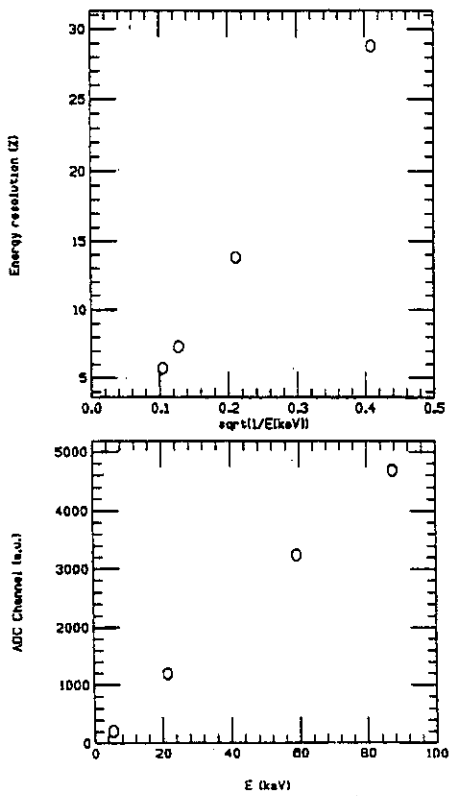

Figure 13: Example of the behaviours of the linearity and energy resolution (σ/E) at low energy: ^{55}Fe (5.9 keV), ^{109}Cd (22 and 88 keV), ^{241}Am (59.5 keV) in one detector.

supported by the results obtained irradiating the whole detectors with high energy γ sources (e.g. ^{137}Cs) from different positions; no appreciable variations of the peak position and energy resolution have been seen.

Finally we remark that our use of single photoelectron threshold for the two PMTs working in coincidence — considering also the relatively high available number of photoelectrons/keV — assures that the coincidence of the two PMTs does not introduce a very significant hardware cut of the events near energy threshold. It results in the present case $\simeq$ 0.8 in the 2-3 keV bin and 1 above 5 keV (depending on the available photoelectrons/keV in the considered detector) for a coincidence time window of 50 ns.

Moreover, a suitable efficiency related to the software procedures used to reject residual noise above the energy threshold has to be measured and used; it will be discussed in some details in the following section.

7 The noise rejection

The NaI(Tl) is a suitable detector for an effective noise rejection, having no contribution from microphonic noise (as it is instead the case of ionizing and bolometer detectors) and being the physical pulses well distinguishable from the noise pulses: essentially the PMT

noise. This effectiveness is higher when a high number of photoelectrons/keV is available, such as in our case. This is an almost unique features and contributes to candidate the NaI(Tl) as a particularly reliable target-detector to study the annual modulation signature.

The rejection of the noise can be performed considering that the scintillation pulses in NaI(Tl) have a time distribution with decay time of order of hundreds ns (typically $\simeq$ 240 ns), while the noise pulses are single fast photoelectrons pulses with decay time of order of tens ns (see fig. 14).

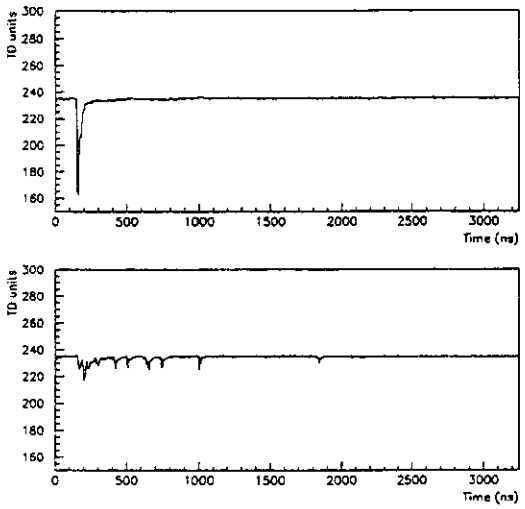

Figure 14: Typical structures of PMT noise (a) and of scintillation (b) pulses, giving the same pulse area above energy threshold.

The different characteristics of these signals can be investigated building several variables, which will follow different distributions for scintillation and noise pulses. As a practical example, we mention here the fraction of the pulse areas evaluated over different time intervals such as $\frac{Area(from\ 100\ ns\ to\ 600\ ns)}{Area(from\ 0\ ns\ to\ 600\ ns)}$ and $\frac{Area(from\ 0\ ns\ to\ 50\ ns)}{Area(from\ 0\ ns\ to\ 100\ ns)}$. For the first variable the noise events are distributed around zero, while the scintillation pulses are distributed around 0.7; the second variable indeed is distributed around one for the noise and around 0.5 for the scintillation events [6]. As mentioned above, the 600 ns time interval corresponds to the typical hardware gate for NaI(Tl) pulses and it is equal to $\simeq$ 2.5 times the decay time of a scintillation pulse, that is the $Area(from\ 0\ ns\ to\ 600\ ns)$ is proportional to the energy of the event.

In fig. 15 a) the typical experimental distributions of the first variable for production data in the 2-20 keV energy region is shown, while in fig. 15 b) the same plot obtained for data collected using an ^{241}Am source in the same 2-20 keV energy interval is shown for comparison.

[6] Qualitatively, hypotizing only one decay constant the expected value for scintillation events should be 0.64 for the first variable and $\simeq$ 0.5 for the second one.

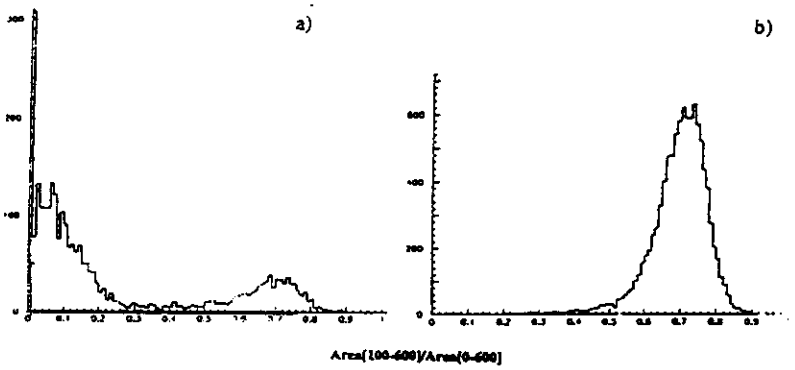

Figure 15: Typical experimental distributions of the variable $\frac{Area(from\ 100\ ns\ to\ 600\ ns)}{Area(from\ 0\ ns\ to\ 600\ ns)}$ in the 2-20 keV energy region: a) for the production data; b) for the data collected using an ^{241}Am source.

In fig. 16 a) and b), both for production data and source data respectively, the two variables are plotted in a bidimensional plot; the signature of the residual noise above the software energy threshold with respect to the scintillation events is evident.

The two populations are well separated and cuts can be applied to effectively reject the residual noise; the corresponding analysis cut efficiencies can be then evaluated and properly used in order to account for good events, that could be cut with the noise near energy threshold[7]. To estimate these analysis cut efficiencies for each considered energy bin, we use the data collected with the ^{241}Am source in the same experimental conditions and energy range (2-20keV) than the production data; stringent cuts can be considered and efficiencies can be properly evaluated (see e.g. the overall behaviour of fig. 17, which is obviously fully dominated by the cut efficiency contribution - see sect. 6).

The lower value at threshold accounts also for the statistical spread of the variables when evaluated from pulses having lower number of photoelectrons [8]. This procedure offers clean samples and correct rates.

It is evident from fig. 15 and 16 that slightly less stringent cuts for noise rejection can be considered, obtaining slightly larger values for the software cut efficiencies; but for analyses searching for effects of order of % near energy threshold (such as annual

[7]We take the occasion to comment that in any kind of experiment for particle Dark Matter direct search software cuts (or - sometimes - hardware procedures) and corresponding correction factors near energy threshold have to be applied.

[8]It is evident that, if — in any other similar experiment — the available number of photoelectrons/keV would be lower and/or the electronic noise from the line would be more important, the effectiveness of the rejection will be poorer.

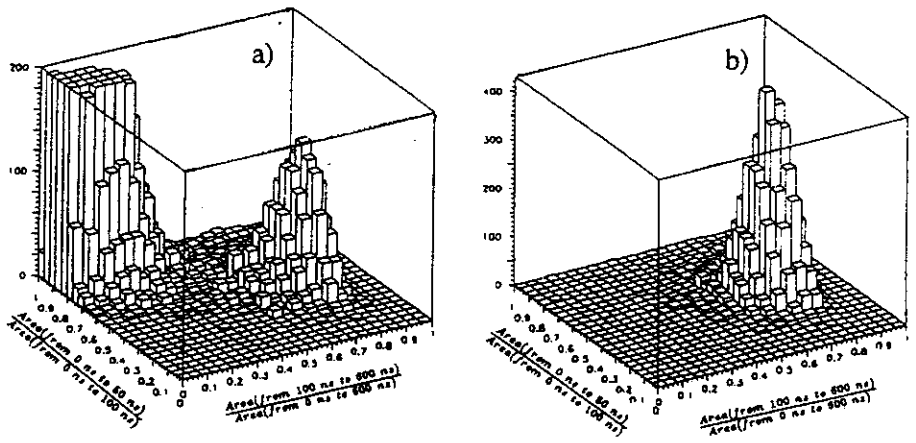

Figure 16: Bidimensional plots for events-noise rejection by using the values of the variables $\frac{Area(from\ 100\ ns\ to\ 600\ ns)}{Area(from\ 0\ ns\ to\ 600\ ns)}$ and $\frac{Area(from\ 0\ ns\ to\ 50\ ns)}{Area(from\ 0\ ns\ to\ 100\ ns)}$ for each event. a) production data in 2-20 keV; b) 2-20 keV data from ^{241}Am source (a and b not normalized). The noise is clearly separated from scintillation pulses.

modulation studies and pulse shape discrimination) very clean samples are necessary to assure the absence of any possible systematics connected with the presence of residual noise contamination. Therefore, considering the large statistics achievable with our set-up, the use of stringent cuts results much more conservative than to release them.

In any case, we want to remark here that obviously when people want to compare efficiency values used in different experiments, these must be averaged on the same energy interval.

Finally, we take the occasion to note that this clear noise identification in NaI(Tl) is almost unique with respect to most of the other kind of detectors used in particle Dark Matter search, where "physical" pulses and noise have often indistinguishable features.

8 Response to neutrons

For the sake of completeness we briefly recall here that measurements have been performed with neutrons in order to experimentally determine the quenching factors for Na and I, q_{Na} and q_I, and the pulse shape discrimination (PSD) capability of the detectors. The first quantities are necessary to properly compare the measured energy spectrum — calibrated with γ sources — with the one expected for WIMP induced recoils, while the study of the PSD can offer a powerful tool to discriminate electromagnetic background from recoils. Experimental details and analysis procedures can be found in ref. [7].

A neutron calibration deep underground is not possible due to the subsequent acti-

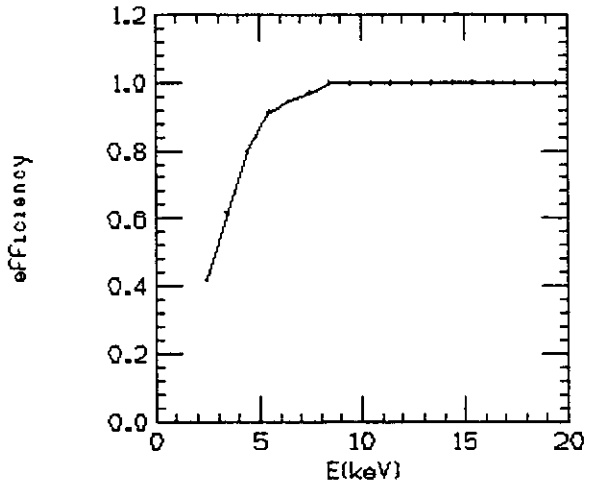

Figure 17: An example of the behaviour of the overall efficiencies (see sect. 6 and 7).

vation of the low radioactive materials. Therefore, we have performed such a calibration at the ENEA-Frascati Laboratory by using a ^{252}Cf neutron source and a crystal with the same features (growing procedure, materials, Tl concentration, assembling, PMT and voltage divider, electronic chain and temperature) as the ones used deep underground [7].

The quenching factor is defined for scintillators as the ratio of the amount of light induced by a recoiling nucleus to the amount of light induced by an electron of the same kinetic energy. In our case a method similar to the one of ref. [17] has been applied to evaluate q_{Na} and q_I, obtaining q_{Na}=0.30 and q_I=0.09 in the energy region of interest for Dark Matter direct search [7]. We stress that this is one of the few cases in which the quenching factors used to achieve physical results have been measured directly in a crystal from the same growth as the ones used deep underground. These measurements allowed also the study of the shape of the nuclear recoil pulses; for this purpose, only events due to neutron single elastic scatterings in the crystal have been selected and considered, analysing the pulse characteristics recorded over 3250 ns by a Lecroy Transient Digitizer. Moreover, to obtain samples of electron induced events, Compton calibrations have been performed *in situ* by using a ^{137}Cs source. We note that, because of the known temperature dependence of the time behaviour for the NaI(Tl) scintillation pulses [9] [10], the calibration crystal has been maintained at the same temperature as the underground set-up, continuously monitoring it within $\pm$ 0.2 ^{0}C.

The collected data have been analysed, considering 2 keV bins between 2 and 20 keV; the statistics ranged from $\simeq$ 2000 up to $\simeq$ 5000 evts/(2keV bin). The time profiles of the pulses, for each energy bin, have been summed both for Compton and neutron runs in order to obtain "reference pulses". The first momentum of the time distribution has been calculated for each of them within 600 ns averaging time, obtaining the τ_{comp} and

[9]For our NaI(Tl) crystals a linear variation with a slope of -3ns/°C has been measured in ref. [7] between 17 and 23 °C; a similar value has been found also in ref. [18], while in the case of ref. [19] -5ns/°C has been empirically estimated and used.

τ_{rec} values, respectively. It resulted that the mean decay time is shorter for single scattering recoils than for the electrons. The discrimination power between electromagnetic ("Compton-like") events and recoils has been then evaluated — as a function of the energy bin — by the relative difference between τ_{comp} and τ_{rec} named discrimination quality factor, DQF: $DQF = [\frac{\tau_{comp}-\tau_{rec}}{\tau_{comp}}]$ (see fig. 18).

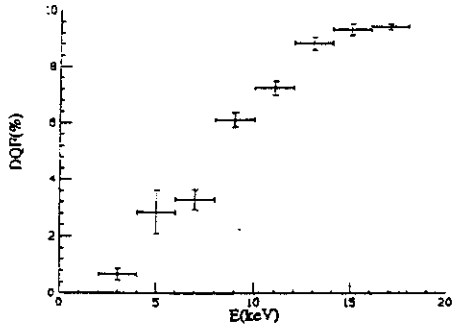

Figure 18: The DQF as a function of the energy bin.

The DQF values offer a quantitative estimate of the electromagnetic background rejection capability and allow the development of an effective PSD strategy (see for details [7]).

9 Monitoring of the running conditions

A continuous on-line control of several parameters is performed in order to monitor the operating conditions of the whole set-up over long periods of data taking. In particular, several quantities and sensors values are sampled and acquired by the CAMAC with the events, such as: i) two reference temperatures; ii) the temperature of the cooling water in the conditioning system of the barrack (for alarm); iii) the HP N_2 flux and the overpressure of the Cu box containing the detectors; iv) the single and total rates above the single photoelectron level (that is from noise to "infinity"). In addition, also the environmental Radon in the barrack is recorded, although the presence of the Supronyl envelop (maintained in HP N_2 atmosphere) which isolates the shield containing the Cu box where the detectors are enclosed and excluded from environmental air (see above).

In fig. 19 the typical behaviours of some of these parameters during the DAMA/NaI-2 long term running period [20] are shown. We recall that — being the installation subject to air conditioning — the environmental temperature cannot be influenced by any external seasonal variations (see for quantitative estimate sect.10).

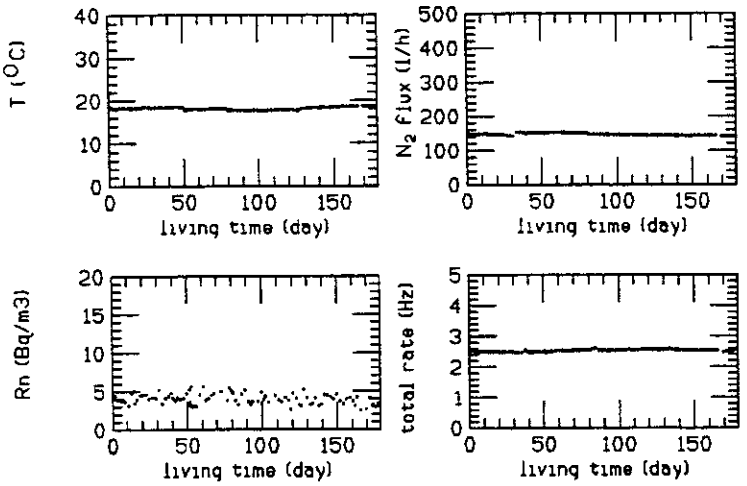

Figure 19: Long period stability of some parameters monitored during the DAMA/NaI-2 running period (see text). Note that total rate means the rate of the OR of the nine crystals above the single photoelectron threshold (i.e. from noise to "infinity") [20].

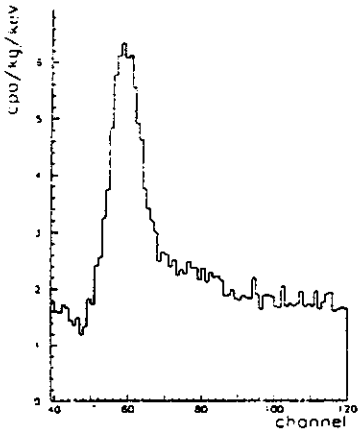

Figure 20: Typical ^{210}Pb peak distribution — summing the data each 7 days — in our NaI(Tl) detectors.

Further "off-line" controls are also performed; in particular, the stability of the energy threshold, of the PMT gain and of the electronic line is verified — in addition to the rates monitoring — by a continuous intrinsic stability control due to the presence of a mainly surface contamination in ^{210}Pb (see above). In fact, the data collected in this energy region are summed every $\simeq$ 7 days (see fig. 20) and the stability both of the

peak position and of the energy resolution is controlled. In fig. 21 a distribution of the relative variations of the energy calibration factors (tdcal) estimated from the position of this peak for all the 9 WIMP detectors over a period of several months (DAMA/NaI-2 running period [20]; see above) is shown.

The information of the ^{210}Pb peak and the ^{241}Am routine calibrations (fig. 22) allows to properly determine the energy scale. Periodical Compton electron calibrations in the 2-20 keV energy region are also performed to be used in the PSD analysis of the events [7]) (see sect. 8).

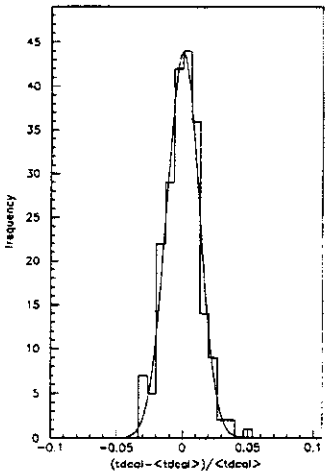

Figure 21: Example of a long period stability from the ^{210}Pb peak for the 9 WIMP detectors (see text); the gaussian fit gives $\sigma = (1.24 \pm 0.08)\%$. The information of the ^{210}Pb peak and the ^{241}Am routine calibrations allows to properly determine the energy scale [20].

Moreover, when searching for the WIMP annual modulation signature, further off-line controls — over the analysed time period — are performed by verifying typical features of the effect searched for [3, 20].

10 Possible systematics

As first we want to comment that sometimes troubles, that are malfunctionings of a set-up, are listed as possible systematics (see e.g. ref. [21]). On the contrary, they must be considered as they are and the use of the affected data set must be discouraged. Therefore, in the following, we will consider only effects which can be source of "real" systematic effects. Furthermore, approaching this discussion, we take the occasion to stress that — as it can be derived from literature — no other set-up for Dark Matter direct search has been previously continuously monitored at the level of the one described here.

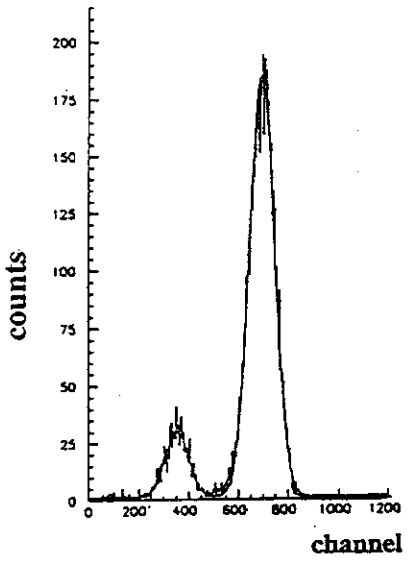

Figure 22: Typical ^{241}Am energy spectrum.

In addition, we stress that systematics is function of the quality of an experiment, therefore its nature and level is generally very different from one experiment to another.

Coming back to the details, we will divide possible systematic contributions in three classes, affecting respectively: i) the case when the counting rate after noise rejection is used to evaluate the exclusion plots; ii) the case when the pulse shape analysis is considered to reject the electromagnetic background in order to achieve more stringent exclusion plots; iii) the case of the annual modulation search to point out a signature for the possible WIMP presence, obviously without considering in this case any PSD of the events[10].

As regards the point i), considering the clear knowlegde and control of the "physical" energy threshold, of the quenching factors, of the efficiencies and of the calibrations with respect to the knowledge of the needed astrophysical (see e.g. table 1 of ref. [22]) and nuclear physics parameters [2], we can conclude that the model uncertainties are — in our case — obviously fully dominant with respect to the possible level of systematics affecting the experimental part. As an example we comment that the quenching factors used in our determinations have been measured directly in a crystal from the same growth with the same assembling as the ones used in the underground installation.

As regards the point ii) a potential systematics can arise from possible difference in the DQF value from a crystal to another, but it has been verified that — when using detectors from the same growth (e.g. with the same Tl percentage) in the same experimental conditions — the DQF remains stable within the errors quoted in ref. [7]. Therefore, the main source of systematics remains the temperature, T, stability during the considered data taking (see also sect. 8): e.g. in our ref. [7] $< T >$=19.11 $\pm$ 0.05 °C. Obviously less

[10] As pointed out several times the PSD has not to be considered for a safe annual modulation study, affecting otherwise with its own uncertainties the effect searched for.

stringent control of the temperature would give rise to larger systematic errors; however, in this case the systematic contribution could be reduced by applying a suitable correction if the slope of the linear τ dependence on temperature — in the interesting energy range — has been previously determined with suitable precision. Another potential source of systematics arises in case of presence of residual PMT noise in the analysed sample of events; in fact, it will modify the τ values of the data "reference pulses" offering lower τ values than the ones expected in absence of recoils, that is simulating the presence of a "recoil-like" population.

Moreover, we take the opportunity to remark that systematic errors in results achieved by applying PSD techniques could also arise from the used analysis strategy itself. As an example, we mention the case when the PSD would be based on the study of the mean photoelectron arrival time, but the gate considered in the evaluations would be too short (that is only a small fraction of the pulse is considered) or too long (that is e.g. afterglows could play a significant role) with respect to the time duration of the scintillation pulse.

Two complete strategies for PSD at low energy in NaI(Tl) have been developed by us in ref. [7] and by the UK collaboration in ref. [18]; as a further example of the role potentially played by the used method in the achievable level of systematic uncertainties we show in table 6 a comparison of these two methods. Our method does not require e.g. any fitting of the recorded pulse[11] and is based on a larger number of photoelectrons/keV.

Table 6: Schematic comparison of the data handling for PSD in ref. [16] and in this experiment [7].

ref. [16]	ref. [7]
1.7 photoelectrons/keV	$\gtrsim$5.5 photoelectrons/keV
fit on single pulse	mean photoelectron arrival time of averaged pulse, τ
fit of the single pulses τ distribution with an empirical formula	
comparison of the fitted free parameter, τ_0, for recoils and Compton with data	comparison of the measured τ values of averaged pulses for recoil and Compton data

As regards the point iii) the important systematics are mainly those who can cancel or simulate the possible presence of a WIMP yearly modulated signal. In fact, the signature for annual modulation is not due to a "generic" rate variation but to a variation according to the following specifications: i) presence of a correlation with cosine function; ii) proper period for the possible modulation (1 year); iii) proper phase for the possible modulation

[11] Note that a pure exponential shape does not represent the single photoelectron structure of the pulse at very low energy.

(about 2 june); iv) in only one well defined energy range; v) for single "hit" events[12]; vi) with modulated amplitude not exceeding $\lesssim 7\%$.

This can be verified by using a suitable analysis strategy, such as the maximum likelihood method used in ref. [3, 20]. This method — working on the differential energy spectrum with 1 keV energy bin[13] — does not require any *a priori* optimization of the considered energy interval to achieve the highest sensitivity. In particular, when a positive indication is achieved the hunt has to be restricted to possible systematics able to fully simulate the signal features. Up to now we find as a possibility — that however should generally fail at least the requirements iv) and v) quoted above — only the muon modulation studied in ref. [23]; however, this could account in any case (considering the features of the WIMP events and of our set-up) roughly only for modulated amplitudes $<< 10^{-4}$ cpd/kg/keV, that is much lower than e.g. the preliminary indication of ref. [3, 20]. In any case, this effect should be considered as a systematics to be faced in future searches for very low modulated amplitude, in case an effect at level of the indication of ref. [3, 20] would not be definitively set.

We take the occasion to comment that the possible presence of short-life decaying isotopes cannot simulate a positive modulation signature if — as in ref. [3, 20] — the data taking period considered in the analysis will start from winter toward summer, that is from a minimum to a maximum of the expected cosine variation of the possible WIMP rate. In the same period the rate of the possible decaying isotope will indeed decrease exponentially. On the other hand if the presence of a decaying isotope would be pointed out, its rate variation could be properly included in the background term during the data analysis.

Finally, we also comment that — in a safe annual modulation search, where the PSD of the events is not used — a sizeable temperature variation could only cause a very small light response variation; around our operating temperature, the average slope of the light output is $\lesssim$ - 0.2%/°C. Therefore, to have a percentage light output variation at level of 2% a variation of 10 °C is needed; that is, the effect is negligible considering the possible level of temperature variations (fraction of °C in our experiment), the energy resolution of the detector in the keV energy region and the role of intrinsic and routine calibrations[14].

[12] when using a multi-detector set-up to search for Dark Matter particles, the quoted rate is always referred to single "hit" events (that is to events where only one detector is firing - see also sect.5), being negligible the probability that a WIMP will interact in more than one detector. For the sake of completeness we note that in our set-up the single-hit rate and the single plus multi-hit rate differ for $\lesssim$ 10%.

[13] This value is a good compromise between an high signal over noise ratio and the statistics available in each energy bin.

[14] Slightly different values for the slope are quoted by different companies, that is in different crystals, such as e.g. + 0.08%/°C by Hilger company, but in any case the effect remains negligible.

11 Conclusion

In this work we have described the main features of the $\simeq$ 100 kg NaI(Tl) set-up of the DAMA experiment searching for particle Dark Matter deep underground in the Gran Sasso National Laboratory of I.N.F.N. It has already achieved several physical results [3, 7, 8, 20].

This experiment plans to search mainly for the WIMP annual modulation signature over several years.

12 Aknowledgements

This realization was performed thanks to the effective support and control of the INFN Scientific Committee II, the continuous support of the INFN sez.-Roma2 and Roma, of the Gran Sasso National Laboratory and IHEP/Beijing. We are also indebt with the referees of the experiment for their competent work, that allowed us several times to improve the quality of our efforts.

We wish to thank Dott. C. Arpesella, Ing. M. Balata , Prof. A. Scacco and Prof. L. Trincherini for their contribution to sample measurements and related discussions. We also thank Prof. I.R. Barabanov and Dr. G. Heusser for many useful suggestions on the features of low radioactive detectors.

We wish also to thank Prof. C. Bacci, Mr. V. Bidoli, Mr. G. Bronzini, Dr. D. Chen, Dr. V. Landoni, Dr. X. Sun, Dr. G.Z. Yao and Dr. Z. Ye for their contribution to the collaboration efforts in various periods and Dr. M. Angelone, Dr. P. Batistoni and Dr. M. Pillon for their effective collaboration in the neutron measurements at ENEA-Frascati.

We thank Dr. R. McAlpine and Dr. T. Wright from EMI-THORN for their competent assistance and the Crismatec company for the devoted efforts in the realization of the NaI(Tl) crystals.

We also wish to thank Mr. A. Bussolotti, G. Ranelli and A. Mattei for qualified technical help and the LNGS, INFN-sezione di Roma and INFN-sezione di Roma2 mechanical and electronical staffs for support.

It is also a pleasure to thank the ACF staff for the effective support in hardware works and assistence.

Finally we are indebt with Prof. S. d'Angelo for his stimulating support to our scientific activities and with Prof. A. Bottino, Dr. F. Donato, Dr. N. Fornengo and Dr. S. Scopel for many useful discussions on the theoretical aspects of the results achieved by our experiment.

References

[1] A.K. Drukier et al., Phys. Rev. D33 (1986), 3495; K. Freese et al., Phys. Rev. D37(1988), 3388.

[2] R. Bernabei, Riv. N. Cim. vol. 18 n. 5(1995).

[3] R. Bernabei et al., Phys. Lett. B424 (1998), 195

[4] G. Alimonti et al., Astrop. Phys. 8(1998), 141.

[5] M. Wojcik, Nucl. Inst. & Meth. B61(1991), 8.

[6] P. Belli et al., Il Nuovo Cim. 101A(1989), 959.

[7] R. Bernabei et al.,Phys.Lett.B389(1996),757.

[8] R. Bernabei et al., Phys. Lett. B408(1997) 439.

[9] Crismatec, private comm.

[10] J.B. Birks, "The theory and the practice of scintillation counting", Pergamon Press Ltd., London (1967).

[11] I.R. Barabanov, priv. comm.

[12] Dyers et al., IEEE91 Th0400-2 (1991), 553.

[13] R. Silberberg and C.H. Tsao, Astrophys.J. 25(1973), 315.

[14] "Table of isotopes" ed. by C. M. Lederer and V. S. Shirley 7-th ed., John Wiley and sons.

[15] A. Fubini et al., Lett. Nuovo Cim. 3 (1970), 785.

[16] G. Ignesti, thesis, in preparation.

[17] K. Fushimi et al. Phys. Rev. C47(1993) R425.

[18] P.F. Smith et al., Phys. Lett. B379(1996), 299.

[19] T. Ali et al., pre-print 1 (january 1998) Imperial College, Atrop. Phys. group, London.

[20] R. Bernabei et al., ROM2F/98/34, August 1998 and INFN/AE-98/20.

[21] N.J. Spooner, talk given at COSMO97, Ambleside, UK.

[22] A. Bottino et al., Phys. Lett. B402(1997), 113.

[23] M. Ambrosio et al., Astropart.Phys.7 (1997), 109.